ADVANCED OPTICAL MATERIALS
www.advopticalmat.de

Broadband Terahertz Metalenses Based on Printed Circuit Board Fabrication

*Chu Qi, Xiaoluo He, Bowen Ren, and Alex M. H. Wong**

Metalenses have provided a good solution to the bulkiness of conventional refractive lenses. Due to the subwavelength feature sizes of the metalens structure, the increasing fabrication difficulties at high frequencies limit its application in the terahertz and optical regime. Moreover, the deeply subwavelength features of the metasurface unit cells usually make the cells strongly resonant, which limits the bandwidth of the metalens. In this paper the usage of aggressive discretization in a metalens design is investigated, and it is found that aggressive discretization can lead to the usage of weakly resonant and relatively large unit cells, which leads to excellent broadband performance and dramatically relaxes the feature size tolerance of the metalens. For examples, two terahertz focusing metalenses are designed which feature large numerical apertures (NA = 0.86), diffraction-limited focusing over a broad bandwidth (240–400 GHz, or 50% bandwidth), and minimum feature sizes of 0.1 mm. These tolerance-relaxed terahertz metalenses are successfully constructed using conventional printed-circuit-board fabrication technology. The experimental measurements validate the simulated performances. Compared to existing terahertz meta-devices based on micro-fabrication or nano-fabrication technologies, this paper opens door to a kind of high-quality terahertz metasurfaces featuring low-cost, rapid, and established fabrication.

1. Introduction

Conventional optical components for focusing and imaging include dielectric refractive lenses and parabolic mirrors. For a conventional dielectric refractive lens, the manipulation of electromagnetic (EM) waves rely on the curvature of the lens surfaces and the phase accumulation provided by the thickness of the lens. Therefore, conventional dielectric lenses are usually bulky. The emergence of the metasurface provides a solution to realize abrupt phase changes with a subwavelength thickness.[1,2] Since then, various metalenses[3–11] and metaholograms[12–21] have been proposed for imaging. The early metalenses based on single-layer plasmonic metasurfaces worked for the cross-polarized component of a linearly polarized incidence, thus suffering from strongly limited efficiency.[4,7,22,23] The metalenses designed based on the Pancharatnam–Berry (PB) phase can achieve a higher efficiency, but they only work for circularly polarized waves.[6,8,11,24–28] A single-layer plasmonic metalens backed with a metallic ground can potentially realize high efficiency. However, their applications are limited to only reflective cases.[5,11,29,30] A transmissive metalens with high efficiency and large numerical aperture (NA) requires unit cells with full transmission phase coverage while maintaining high transmission magnitude, which cannot be realized with single-layer plasmonic metasurface element.[3] Metalenses based on multi-layer plasmonic element structures have been proposed to realize efficient manipulation of the co-polarized component of a linearly polarized incidence.[31–37] However, the metallic patterns of most multi-layer metallic metasurfaces have feature sizes much smaller than the unit cell size, which themselves are often deeply subwavelength. They are thus difficult to fabricate when the frequency goes beyond the millimeter wave (MMW) band. In the terahertz (THz) and optical regimes, dielectric metalenses have been proposed to achieve efficient control of different EM polarizations.[10,38–45] However, due to the resonant nature of the dielectric unit cells, the dielectric metalenses usually have narrow operation bands.

In parallel to these achievements, we have presented the aggressively discretized metasurface, which is designed to have the least number of unit cells required for the desired diffraction mode control.[46] With aggressive discretization, the metasurface unit cells can be greatly enlarged without limiting the

C. Qi
College of Physics and Electronic Engineering
Sichuan Normal University
Chengdu 610068, China
C. Qi, X. He, B. Ren, A. M. H. Wong
Department of Electrical Engineering
City University of Hong Kong
Hong Kong SAR, China
E-mail: alex.mh.wong@cityu.edu.hk
A. M. H. Wong
State Key Laboratory of Terahertz and Millimeter Waves
City University of Hong Kong
Hong Kong SAR, China

The ORCID identification number(s) for the author(s) of this article can be found under https://doi.org/10.1002/adom.202302459

DOI: 10.1002/adom.202302459

performance of the metasurface. This leads to simple structures with significantly enlarged feature sizes. The enlargement of feature sizes can make possible metasurface designs at high frequency range. In a previous work, our group has presented an anomalous refraction metasurface designed on printed circuit boards (PCBs), the aggressive discretization result in a critical feature size of 0.15 wavelength. Considering the conventional PCB fabrication with a typical precision of 0.1 mm, this large feature size can be easily realized fabricated even when the frequency goes up to 450 GHz, which reaches the lower end of the THz spectrum. This shows that, with aggressive discretization, THz metasurfaces may be designed and fabricated on PCBs, which potentially leads to high efficiency and low-cost lenses for THz imaging applications.

In this work, we design and fabricate two transmissive focusing THz metalenses (at 300 GHz) with conventional PCB technology. First, unit cells with three cascaded rectangular strips are designed to realize efficient focusing of a linearly polarized plane wave. Further, by replacing each rectangular strip with a cross-shaped patch, polarization-insensitive unit cells are designed for a dual-polarized focusing metalens. In both cases, we use the concept of aggressive discretization to design unit cells with maximized feature sizes, without compromising the lens' imaging performance. Both metalenses are designed with a size of 20 × 20 mm^2 and a focal length of 6 mm at 300 GHz, thus achieving a large numerical aperture of 0.86. Besides, the proposed metalenses can realize diffraction-limited focusing within a broad bandwidth of 240–400 GHz. Due to the simple structure of the elements, the metalenses are both designed with a minimum line width and gap distance of 0.1 mm, which can be fabricated straightforwardly using a standard PCB fabrication process. Both metalenses are fabricated and measured, and the experimental results agree well with the simulation results. Compared to most of the micro and nanofabrication techniques used in previous THz lens designs, the standard PCB fabrication process is cost-effective and ready for mass fabrication.

2. Metalens Design and Simulated Performances

In this section, we first investigate the effect of aggressive discretization in a metalens design. Then we apply aggressive discretization to design a focusing metalens using a linearly polarized unit cell structure. After that, we extend the single polarized metalens to a polarization-insensitive metalens. Due to the large unit cell size, both metalenses can be designed with a minimum feature size of 0.1 mm, which can be fabricated using a standard PCB fabrication process.

2.1. Aggressive Discretization of a Metalens

We investigate the discretization of a metalens by examining the scattered wave contents in the spectral domain (*k*-space). **Figure** 1a shows the *k*-space operation of a metasurface illuminated by a plane wave with an incidence angle θ_i and a tangential wavenumber $k_i = k_0 \sin\theta_i$. k_0 is the free space wavenumber. The metasurface varies along y-direction. The output spectrum (i.e., the distribution of the transmitted/reflected EM wave in the spatial frequency (k_y) domain) is determined by the input spectrum and the metasurface response spectrum. In the output spectrum, only the modes within the propagation range (i.e., $k_y \in [-k_0, k_0]$) can scatter into the far field; the other modes are evanescent. The directions of the scattered waves are determined by the corresponding tangential wavenumbers. Figure 1b shows the schematic diagram of the transmissive metasurface in Figure 1a. Figure 1c is a schematic showing the directions of the scattered waves, corresponding to the output spectrum in Figure 1a. The transmission/reflection angle corresponding to the *n*th mode is:

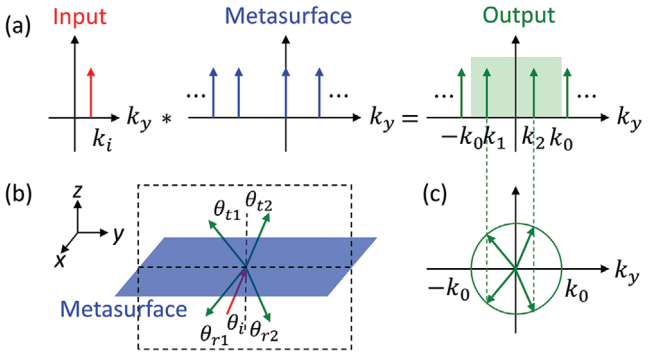

Figure 1. a) *k*-space operation of a metasurface which varies along y-direction. The asterisk sign (*) denotes the convolution operation. Arrows indicate the existence of modes with different tangential wavenumbers. The green box in the output spectrum denotes the propagation range of $k_y \in [-k_0, k_0]$. b) A schematic diagram of a transmissive metasurface upon an incidence with incidence angle θ_i. c) A diagram showing how the output spectrum in (a) corresponds to the directions of the scattered waves.

$$\theta_{tn} = \theta_{rn} = \sin^{-1}\left(\frac{k_n}{k_0}\right) \tag{1}$$

The discretization of a metasurface can be investigated by studying its *k*-space spectrum. A metasurface can be treated as an array of equi-spaced scatterers with similar scattering patterns. Using Fourier transform theory, one can obtain the scattered wave contents (in the spectral domain) generated by the discrete scatterers (in the spatial domain). To be specific, if we know the transmission (reflection) characteristics of the scatterers, we can find the *k*-space spectrum of transmission (reflection) coefficient profile of the metasurface.

The discretization of a periodic metasurface has been studied in a previous work.[46] A metalens is an aperiodic arrangement of discrete elements. As guaranteed by the Fourier transform theory, the corresponding *k*-space spectrum will be continuous and periodic. If the element size of the discrete metalens is U, its *k*-space spectrum will be periodic with a period of $\frac{2\pi}{U}$. Generally, metalenses may deal with scattered waves radiating in all directions, especially for metalenses with large NAs. That means the waves scattered by a metalens may have the tangential wavenumbers covering the whole propagating range of $[-k_0, k_0]$. In this case, to avoid aliasing in *k*-space, the *k*-space periodicity should be larger than the free-space propagation range, that is, $\frac{2\pi}{U} \geq 2k_0$, resulting in a maximum element size of $U = 0.5\lambda_0$. A more detailed study of metalens discretization can be found in the Section S1, Supporting Information. The conclusion is that one can

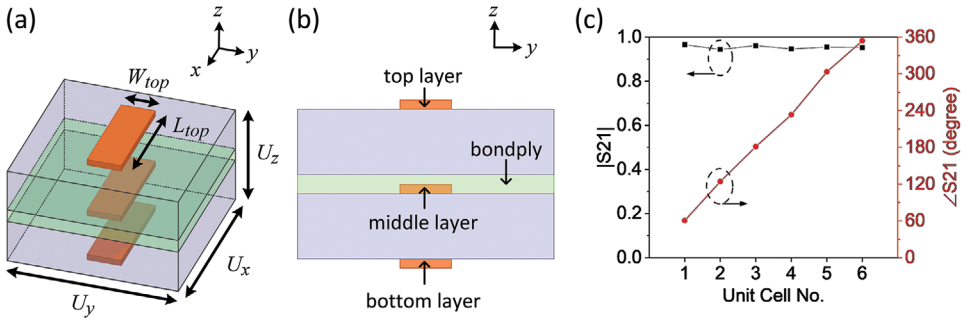

Figure 2. a) Perspective view and b) front view of the unit cell. c) The transmission magnitudes and phases of the six unit cells composing the proposed metalens at the design frequency of 300 GHz.

construct a metalens with an element size as large as $U = 0.5\lambda_0$ without suffering aliasing effects in the angular domain. This has significance on building metalenses with low tolerance requirements.

2.2. Metalens Design

We design the focusing metalens following the hyperbolical phase profile which can be expressed as[47]

$$\Delta\varphi\ (x, y) = \frac{2\pi}{\lambda_0}\left(\sqrt{x^2 + y^2 + F^2} - F\right) \tag{2}$$

where $\Delta\varphi(x, y)$ is the required phase difference between the position (x, y) and the center point (0,0) of a flat lens placed on the xy plane, λ_0 is the working wavelength and F is the focal length. The focusing ability of a metalens depends on the numerical aperture (NA), which is:

$$\mathrm{NA} = \sin\left(\tan^{-1}\frac{D}{2F}\right) = \frac{D}{2}\left(\frac{D^2}{4} + F^2\right)^{-\frac{1}{2}} \tag{3}$$

where D is the diameter of the metalens. The performance of a metalens with a large NA may suffer from angular dispersion of the unit cells at the edge of a metalens, since these unit cells should deflect a wave from normal to a refraction angle of $\theta = \sin^{-1}\mathrm{NA}$, which becomes large as NA increases. In a previous work[46] we have shown that the unit cell with three cascaded metallic strips can work well with incidence and refraction angles within $\pm$ 60°, therefore, we believe the metalens based on this unit cell structure can achieve an NA $\approx \sin 60° = 0.866$. We design the focusing metalens with a focal length of $F = 6\lambda_0$ and a dimension of $D = 20\lambda_0$. The NA of the proposed metalens, calculated using Equation (3), is 0.86. We design the metalens with a discrete unit cell size of $0.5\lambda_0$ and a phase quantization level of six.

We design a linearly polarized metalens using a triple-layer microstrip unit cell shown in **Figure 2**a,b, which we first used in our previous work.[46] While other broadband unit cell topologies are possible, in this work we have chosen this unit cell because it possesses i) simple geometric features, ii) a wide-angle and broadband response, and iii) a co-polarized scattering property that can be expanded to dual-polarization or polarization-insensitive operation, as we shall show later in the paper. The chosen unit cell is constructed using three layers of rectangular strips with length L and width W. The size of the unit cell is $U_x = U_y = 0.5\lambda_0$, which is 0.5 mm at the design frequency of 300 GHz. The metalens is designed on two Rogers RT/duroid 5880 boards ($\epsilon_r = 2.2$, $\delta_t = 0.0009$) bonded by a Rogers 2929 bondply ($\epsilon_r = 2.94$, $\delta_t = 0.003$). The Rogers RT/duroid 5880 boards have a substrate thickness of 0.127 mm and a copper cladding thickness of 17.8 µm. The thickness of the Rogers 2929 bondply is 0.038 mm. By sweeping the lengths and widths of the three strips, we can obtain unit cells with different transmission coefficients. It should be noted that the unit cell parameters are swept and tuned under the condition that the minimum feature size (line width and gap distance) of the metalens is 0.1 mm, so that the proposed metalens can be fabricated with a standard PCB etching process. Having obtained the unit cells with sufficient transmission phase coverage, we choose six unit cells with equidistant transmission phases while maintaining similar high transmission magnitudes to construct the metalens. Figure 2c shows the transmission magnitudes and phases of the six unit cells, with their geometrical parameters given in **Table 1**. CST Studio Suite is used to simulate the proposed metalens. The metalens is placed on the xy plane with its center position at $(x,y,z) = (0,0,0)$. It is illuminated by an x-polarized plane wave propagating along the $+z$-direction from the bottom. **Figure 3**a shows the perspective view of the proposed metalens with normalized intensity distributions at the design frequency of 300 GHz. From Figure 3a we can observe the focusing effect with a focal length of 6 mm as designed.

2.3. Performance within BROAD Bandwidth

In this section we examine the performance of the metalens over a broad operation bandwidth.

We expect the metalenses we design leveraging aggressive discretization would exhibit stable broadband performance for the following reasons. First, aggressive discretization allows one to use large metasurface elements of up to $U = 0.5\lambda_0$, which in turn allows the use of the simple structures with large feature sizes. Second, these simpler structures can be built to be weakly resonant, thus minimizing loss and avoiding abrupt changes in scattering response with respect to changes in frequency. Third,

Table 1. Geometrical parameters of the unit cells.

Unit cell no.	L_{top} [mm]	W_{top} [mm]	L_{mid} [mm]	W_{mid} [mm]	L_{bot} [mm]	W_{bot} [mm]
1	0.30	0.15	0.21	0.22	0.30	0.22
2	0.25	0.15	0.20	0.25	0.25	0.20
3	0.15	0.15	0.20	0.10	0.10	0.20
4[a)]	0.10	0.10	0.50	0.15	n/a	n/a
5	0.50	0.10	0.50	0.15	0.50	0.10
6	0.50	0.19	0.50	0.12	0.50	0.19

[a)] The 4th unit cell has no metallic pattern on the bottom layer.

the large element size also alleviates the strong mutual coupling which is often observed among deeply subwavelength metasurface elements. These advantages combine to lead to stable performance of the metalens.

Our simulation results validate the metalens operation over a broad bandwidth from 240 to 400 GHz (a 50% bandwidth). From Equation (2) we can see, with an invariable transmission phase profile, the focal length (F) will generally increase with decreasing working wavelength (λ_0). That is, assuming the unit cells' transmission phases remain constant, or that they all shift similarly with the illumination frequency, the metalens will have a longer focal length with increasing frequency. Figure 3b plots the focal length and NA as a function of working frequency. When the frequency increases from 240 to 400 GHz, the focal length gradually increases from 3.4 to 9.8 mm. From Equation (3) we can see that an increasing focal length will lead to a decreasing NA. When the frequency increases from 240 to 400 GHz, the NA of the proposed metalens decreases from 0.95 to 0.71, which is still high compared to the previous THz metalens designs.[7,22,28,31,36,37,45] Figure 3d,e plot the normalized intensity distributions along y and x directions across the focal center on the focal plane, showing a good focusing effect with sidelobes lower than 0.1 (−10 dB). Figure 3c plots the spot size (full-width-at-half-maximum (FWHM)). $FWHM_x$ and $FWHM_y$ are the FWHM in the x and y directions respectively. The smaller $FWHM_y$ is due to a smaller angular dispersion of the unit cells for the transmitted wavevector components on the yz plane than that for the wavevector components on the xz plane. Due to the

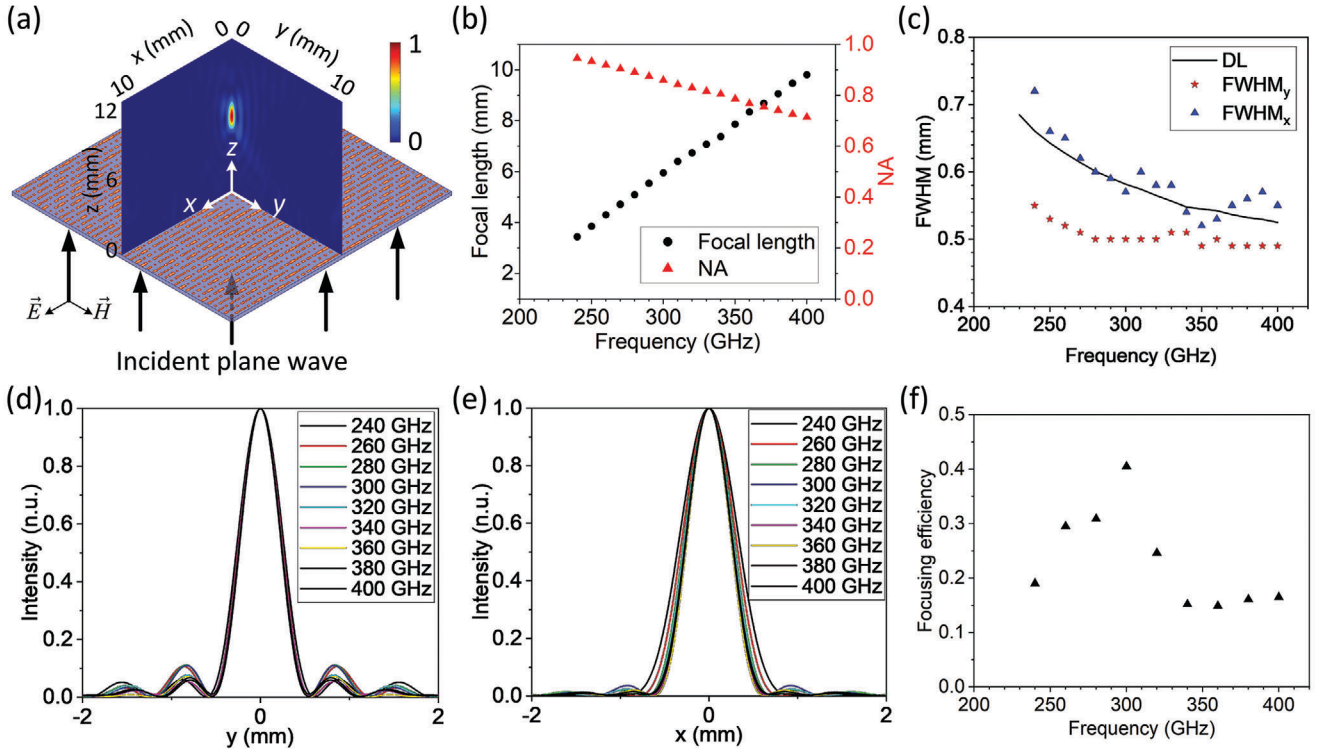

Figure 3. a) Perspective view of the proposed metalens with normalized intensity distribution showing the focusing effect. b) Focal length and NA of the proposed metalens as a function of the working frequency. c) FWHM of the focal spot compared to the corresponding diffraction limit (DL). d,e) Normalized intensity distributions along the y-direction ($x = 0$) and x-direction ($y = 0$) on the focal plane upon incidences with different frequencies. f) Focusing efficiency of the proposed metalens.

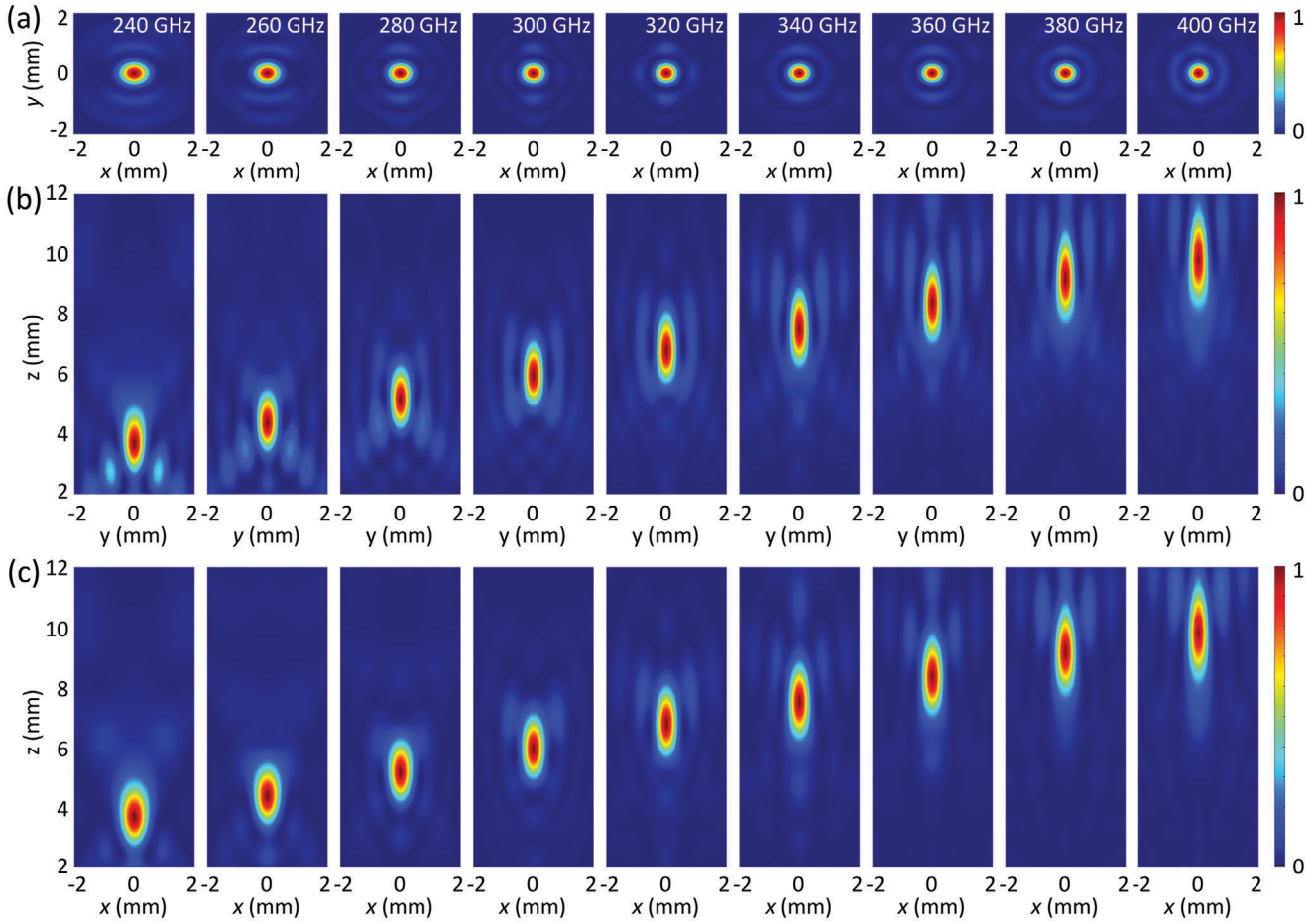

Figure 4. Normalized intensity distributions on a) the focal plane: *xy* plane with z = focal length, b) the *yz* plane with $x = 0$, and c) the *xz* plane with $y = 0$, when the metalens is illuminated by plane waves with different frequencies ranging from 240 to 400 GHz.

physics of wave diffraction, the resolution of conventional optics is limited by the Abbé's diffraction limit (DL), which is related to the NA as[48]

$$\mathrm{DL} = \frac{0.5\lambda_0}{\mathrm{NA}} \tag{4}$$

Nevertheless, within the bandwidth of 240–400 GHz, the focal spot of the proposed metalens has an FWHM very close to the corresponding DL in both directions, realizing broadband diffraction-limited focusing. The focusing efficiency is also used to characterize the focusing performance of a metalens, it is defined as the ratio between the power passing through the area with a size equal to six times the FWHM on the focal plane and the incident power.[40] Figure 3f plots the focusing efficiency of the proposed metalens. We can see the focusing efficiency reaches the highest (40%) at the design frequency of 300 GHz, while remaining above 15% within the frequency band of 240–400 GHz. **Figure 4** shows the normalized intensity distributions of the proposed metalens upon incident plane waves at different frequencies, from which we can observe good focusing performance as well as the focal length changing within the frequency range of 240–400 GHz.

2.4. Performance upon Oblique Incidence

Figure 5 shows the performance of the proposed metalens upon oblique incidence. Upon incident plane waves from directions (θ_i,ϕ_i) with $\theta_i \leq 30°$, $\phi_i = \{0°, 90°\}$, the focal length remains at around 6 mm. The intensity distributions on the focal plane (*xy* plane at z = 6 mm) are plotted in Figure 5a,b. They show the focal spot shifting according to the incident angle. For oblique incidence on the *yz* plane ($\phi_i = 90°$), the focal spot shifts along the y-direction, as shown in Figure 5a; for oblique incidence on the *xz* plane ($\phi_i = 0°$), the focal spot shifts along the x-direction, as shown in Figure 5b,c plots the positions of the focal spots with different incident directions. Figure 5d shows the FWHMs of the focal spots. Both FWHM_x and FWHM_y increase with increasing θ_i, showing a slightly worsened focusing performance with increasing θ_i. For incidences with $\phi_i = 90°$ ($\phi_i = 0°$), The FWHM_y (FWHM_x) of the focal spot changes slightly, while FWHM_x (FWHM_y) increases more significantly. Nevertheless, upon the incidences with θ_i up to 30°, the metalens maintains respectable focusing performance, generating spot sizes with FWHMs smaller than the illumination wavelength of 1 mm.

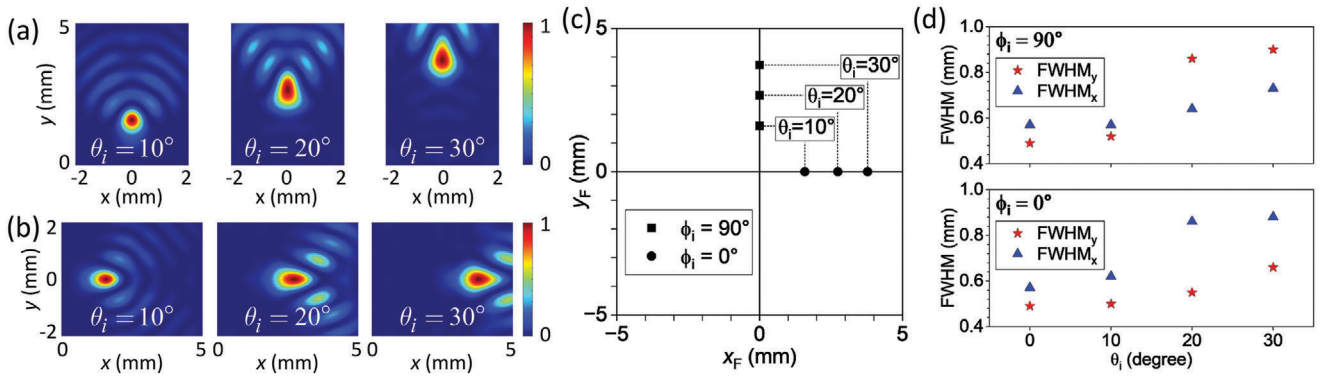

Figure 5. Performance of the proposed metalens upon oblique incidences. Normalized intensity distributions on the *xy* plane ($z = 6$ mm) with a) $\phi_i = 90°$ (oblique incidence on the yz plane) and b) $\phi_i = 0°$ (oblique incidence on the *xz* plane). c) The focal position on the *xy* plane ($z = 6$ mm). d) The FWHM of the focal spots.

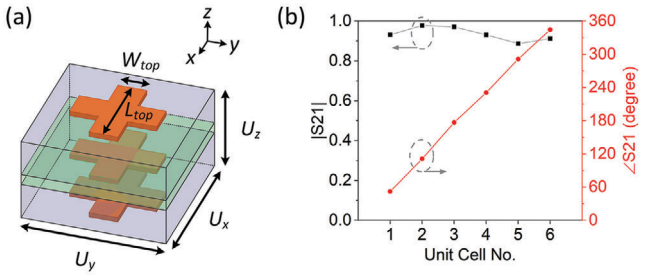

Figure 6. a) Perspective view of the polarization-insensitive unit cell. b) The transmission magnitudes and phases of the six unit cells composing the polarization-insensitive metalens at the design frequency of 300 GHz.

2.5. Polarization-Insensitive Metalens

We extend the metalens design to work for both polarizations by replacing each rectangular strip with a cross-shaped patch in the unit cell structure, as shown in **Figure** 6a. With the same design procedure, we arrive at a polarization-insensitive metalens design. Figure 6b shows the transmission magnitudes and phases of the six unit cells, with their geometrical parameters given in **Table** 2. **Figure** 7a shows the perspective view of the proposed polarization-insensitive metalens with normalized intensity distribution at 300 GHz, showing the focusing effect.

The polarization-insensitive metalens also works well in a broad frequency bandwidth from 240 to 400 GHz (a 50% bandwidth). Figure 7b plots the focal length and NA of the metalens with changing frequency. Figure 7c compares the focal spot width to the Abbé diffraction limit, clearly the spot size is diffraction limited across the wide bandwidth stretching from 240–400 GHz. The smaller $FWHM_y$ is due to a smaller angular dispersion of the unit cells for the transmitted wavevector components on the *yz* plane than that for the wavevector components on the *xz* plane. Figure 7d,e plot the normalized intensity distributions along *y* and *x* directions across the focal center on the focal plane, showing a good focusing effect with sidelobes lower than 0.1 (−10 dB). The intensity distribution generated by the metalens can be found in the Section S2, Supporting Information. Figure 7f plots the focusing efficiency of the proposed metalens. We can see the focusing efficiency reaches the highest (43%) at the design frequency of 300 GHz, while remaining above 14% within the frequency band of 240–400 GHz.

Figure 8 shows the performance of the proposed polarization-insensitive metalens upon oblique incidence. Upon incident plane waves from directions (θ_i,ϕ_i) with $\theta_i \le 30°$, $\phi_i = \{0°, 90°\}$, the focal length remains at around 6 mm. Figure 8a,b plots the normalized intensity distributions on the focal plane and show how the focal spots shifting with the incidence angle. The positions of the focal spots with different incident directions are plotted in Figure 8c,d shows the FWHMs of the focal spots. As expected, the spot size increases with increasing θ_i. Nonetheless, the FWHM remains smaller than the working wavelength of 1 mm when θ_i increases to 30°, showing respectable focusing performance under oblique incidence.

Table 2. Geometrical parameters of the unit cells composing the polarization-insensitive metalens.

Unit cell no.	L_{top} [mm]	W_{top} [mm]	L_{mid} [mm]	W_{mid} [mm]	L_{bot} [mm]	W_{bot} [mm]
1	0.32	0.10	0.22	0.22	0.34	0.10
2	0.22	0.22	0.22	0.22	0.30	0.10
3	0.22	0.22	0.10	0.10	0.10	0.10
4	0.12	0.12	0.50	0.18	0.12	0.12
5	0.50	0.10	0.40	0.10	0.10	0.10
6	0.50	0.12	0.38	0.10	0.50	0.12

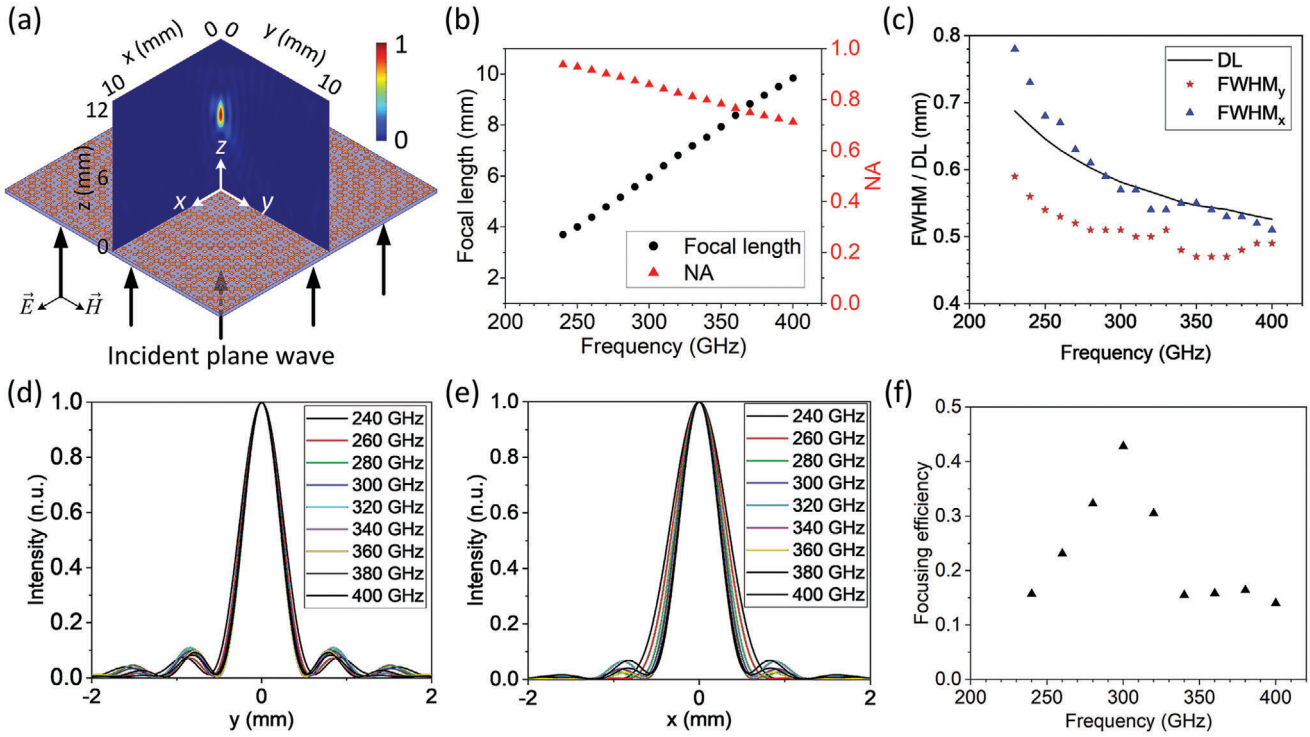

Figure 7. a) Perspective view of the proposed polarization-insensitive metalens with normalized intensity distribution showing the focusing effect. b) Focal length and NA of the proposed polarization-insensitive metalens as a function of the working frequency. c) FWHM of the focal spot compared to the corresponding DL. d,e) Normalized intensity distributions along the *y*-direction ($x = 0$) and *x*-direction ($y = 0$) on the focal plane upon incidences with different frequencies. f) Focusing efficiency of the proposed polarization-insensitive metalens.

3. Experimental Results

We have fabricated and measured the proposed metalenses. **Figure** 9a,b shows the top and bottom layers of the fabricated metalenses. Conventional PCB fabrication is performed on a Rogers substrate and bond wire material system as introduced in Section 2. The feature size tolerance guaranteed by the manufacturer was 0.1 mm. The size of each metalens is 20 × 20 mm^2, at the center of a 30 × 30 mm^2 PCB board. For both lens fabrications, a 5 mm metallic margin is left on the bottom layer for lens support assembly as well as blocking the direct transmission of power from the feed horn to the probe. Figure 9c shows the experimental setup for the near-field scanning measurement. Two pairs of millimeter-wave VNA extenders, OML V03VNA2-T/R, and V02.2VNA2-T/R, are used to extend the operating frequency of the VNA (Agilent N5245A) to THz frequency bands of 220–325 and 325–500 GHz respectively. For each case, one extender is connected to a feed horn (Millitech SGH-03 for 220–325 GHz, Virginia Diodes WR2.2H for 325–500 GHz) while the other extender is placed on a three-axis translational stage and connected to a scanning probe (VIVA Tech WR03 Probe for 220–325 GHz, VIVA Tech WR2.2 Probe for 325–500 GHz). The

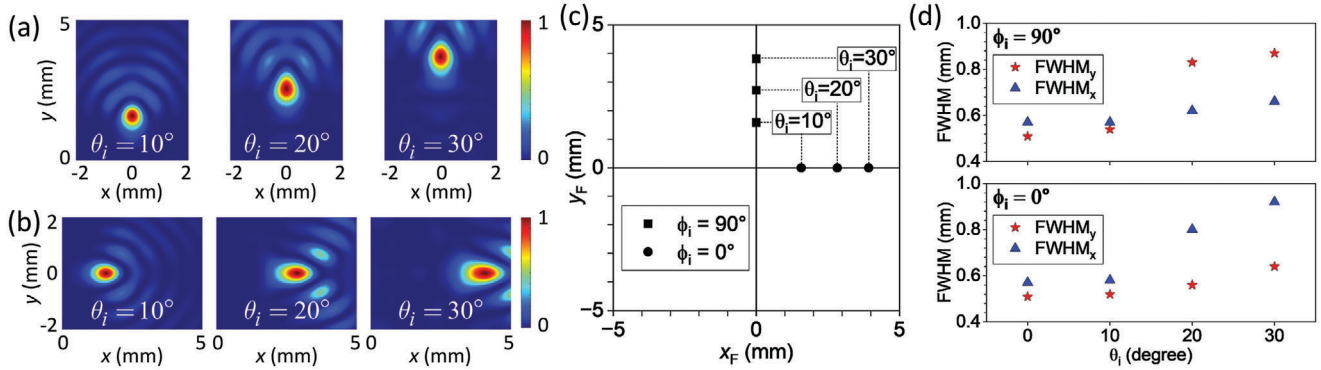

Figure 8. Performance of the proposed polarization-insensitive metalens upon oblique incidences. Normalized intensity distributions on the *xy* plane ($z = 6$ mm) with a) $\phi_i = 90°$ (oblique incidence on the *yz* plane) and b) $\phi_i = 0°$ (oblique incidence on the *xz* plane). c) The focal position on the *xy* plane ($z = 6$ mm). d) The FWHM of the focal spots.

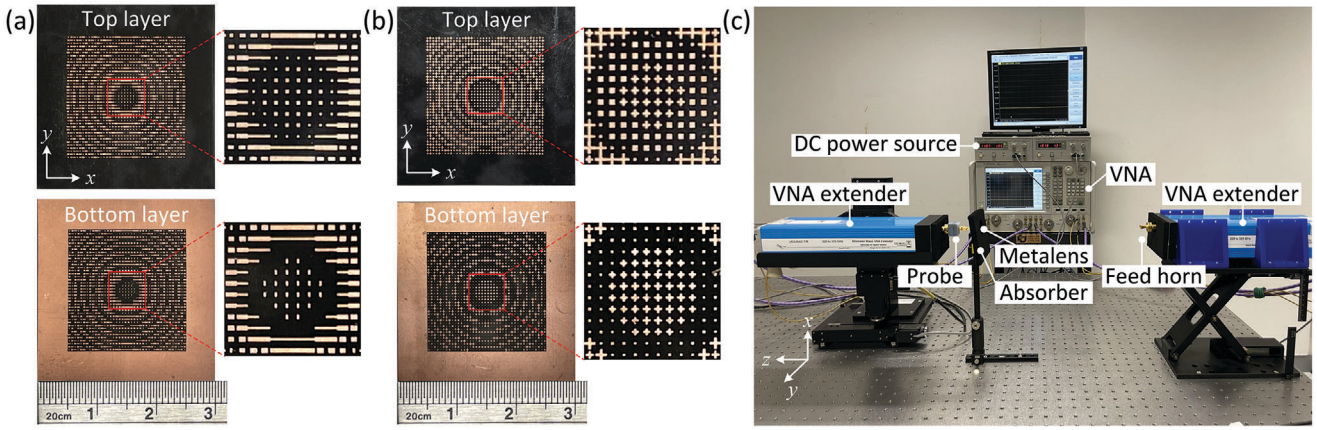

Figure 9. Photographs of a) The fabricated linear polarized metalens. b) The fabricated polarization-insensitive metalens. c) The experimental setup.

metalens is placed on a support placed between the feed horn and the probe. The extenders and the metalens support are placed on an optical table (Newport S-2000 Stabilizer) to ensure stability. The experimental results are obtained by scanning the probe to measure the electric field distributions on the corresponding planes with a scanning step of 0.1 mm.

3.1. Linear Polarized Metalens

Figure 10 plots the measured intensity distributions. Figure 10a–c shows the normalized intensity distributions on the focal (xy) plane, yz plane ($x = 0$), and xz plane ($y = 0$) respectively, at different frequencies from 240 to 400 GHz. Figure 10d,e shows the normalized intensity distributions on the focal (xy) plane upon oblique incidences. The measured intensity distributions agree well with the simulated ones shown in Figures 4 and 5a,b. In **Figure 11**, we compare the measured results to the simulated ones. Figure 11a,b shows the normalized intensity distributions along the y and x directions across the focal center on the focal plane, from which we can find the FWHMs. From Figure 11d, we can see that the measured FWHMs are close to the metalens DL. Compared to the simulated FWHMs, the measured FWHMs are in general slightly larger and the sidelobes are in general lower compared to the simulation results as shown in Figure 11a,b. Figure 11c plots the focal length as a function of the working frequency. Figure 11e plots the focal position of the proposed metalens upon oblique incidences at 300 GHz. From the comparison we can see, the measured results are in good agreement with the simulated results.

3.2. Polarization-Insensitive Metalens

Figure 12 plots the measured results of the polarization-insensitive metalens within the frequency range of 240–320 GHz. Unfortunately, we could not make measurements beyond 320 GHz because the VNA extender for the higher frequency band was out of service at the time of our experiment. Nevertheless, the comparison between the measured and simulated results in the measured frequency band shows good agreement. Figure 12a plots the normalized intensity distributions of the co-polarization (Co-pol) and cross-polarization (X-pol) on the focal (xy) plane, showing efficient focusing performance for the Co-pol and minimal unwanted conversion to the X-pol. Figure 12b,c plots the normalized intensity on the yz plane ($x = 0$) and xz plane ($y = 0$), showing the expected shift of the focal length with frequency. The focal length as a function of frequency is plotted in Figure 12h. A strong agreement with simulation is achieved. Figure 12d,e shows the normalized intensity distributions along the y and x directions across the focal center on the focal plane, from which we can find the FWHMs. Figure 12i plots the FWHMs. The measured FWHMs are slightly larger than the simulated ones, nevertheless, they remain close to the DL. Figure 12f,g plots the normalized intensity distributions on the focal (xy) plane upon oblique incidences, showing how the focal spot shifts with the change of incidence direction. The positions are plotted in Figure 12j.

3.3. Focusing Efficiency

We also measured the focusing efficiencies of the fabricated metalenses at 300 GHz. We perform this measurement by integrating the focal plane intensity over an area of six times the measured FWHM, then dividing by the incident power. The incident power is measured by integrating the intensity over the entire observation plane (with a size equal the metalens size) without the metalens. The measured focusing efficiencies are 15% and 17% for the linear polarization and polarization-insensitive metalenses respectively. The measured focusing efficiencies are comparable to previous THz focusing metalenses, which report measured focusing efficiencies from 1%[23] to 24%.[45] However, the measured focusing efficiencies are lower than the simulated values. In the Discussion Section 4.1, we will investigate the reasons leading to the discrepancy between the simulated and measured efficiencies and suggest viable methods to improve the experimental focusing efficiency despite experimental imperfections.

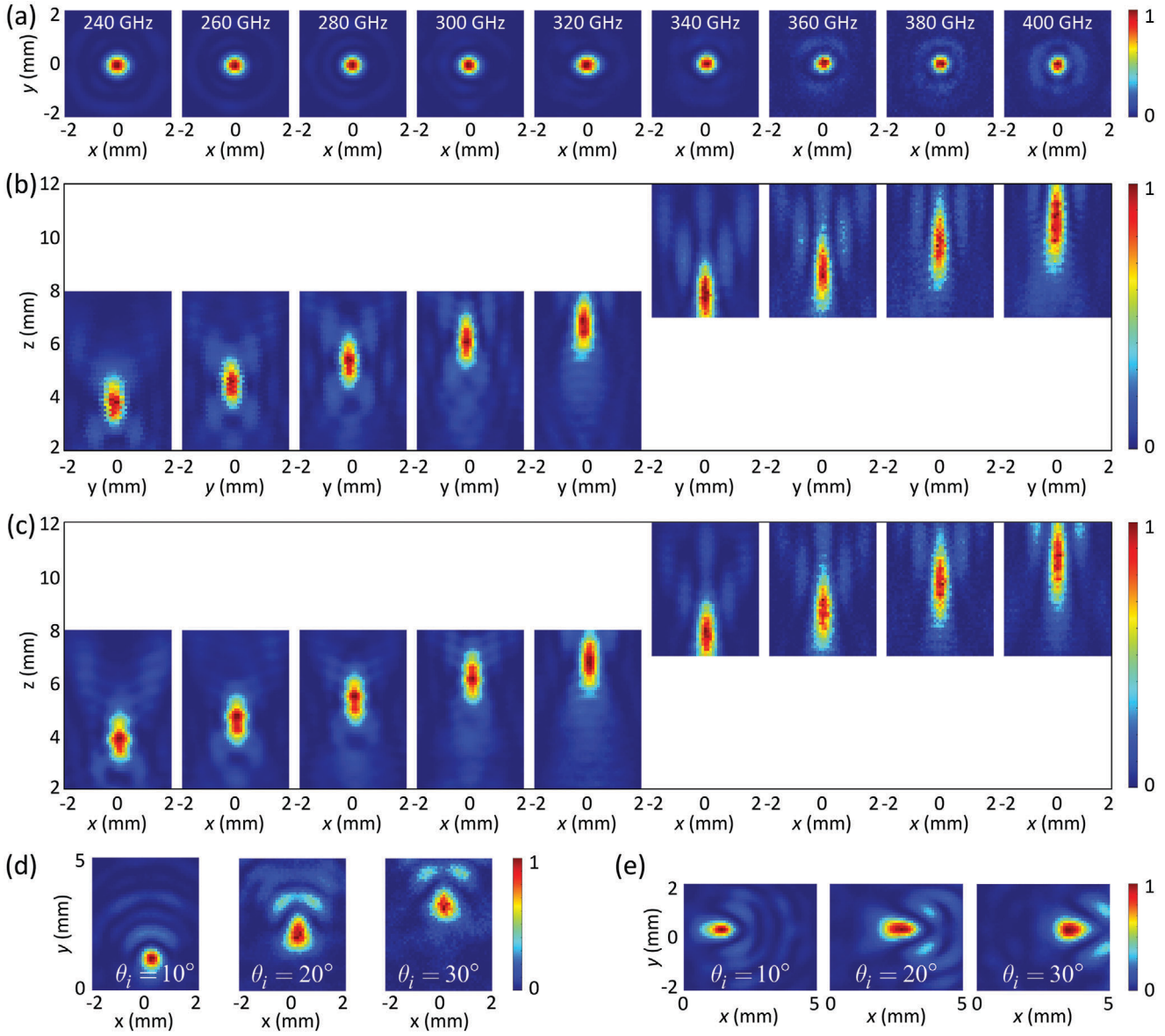

Figure 10. Measured intensity distributions. The normalized intensity distributions on a) the focal (xy) plane (z equals to the measured focal length as plotted in Figure 8c), b) the yz plane ($x = 0$), c) the xz plane ($y = 0$) at different frequencies. The normalized intensity distributions on the focal (xy) plane ($z = 6$ mm) with oblique incidences with d) $\phi_i = 90°$ and e) $\phi_i = 0°$. In (b) and (c), the measured z range is 2–8 mm for the frequency range of 240–320 GHz, and 7–12 mm for the frequency range of 340–400 GHz.

4. Discussion

4.1. Discussion on Focusing Efficiency

In this section we provide analysis results explaining the difference between the simulated and measured focusing efficiencies, and thereafter suggest methods to improve the experimental focusing efficiency. Several reasons may lead to the discrepancy between the simulated and measured efficiencies, including dielectric properties change, conductor surface roughness, fabrication error, among other reasons. Through the investigation, we find that the discrepancy between the simulated and measured efficiencies is mostly due to the dielectric materials (substrate and bondply) having different material properties at 300 GHz than what we assumed in our design. The simulation results with different dielectric material properties can be found in Section S3, Figures S3, and S4, Supporting Information. Therefore, we think that, as long as we know the property of our materials at 300 GHz, PCB based meta-devices (including metalenses) designed from the aggressive discretization concept can still achieve high efficiencies. To prove this point, we design and simulate a linearly polarized metalens with the changed dielectric material properties of $\epsilon_r = 2.3$, $\delta_t = 0.02$ for the substrate and $\epsilon_r = 3.07$, $\delta_t = 0.07$ for the bondply. The unit cells' geometrical parameters are given in Table S1, Supporting Information. The simulated focusing efficiencies are plotted in Figure S5, Supporting

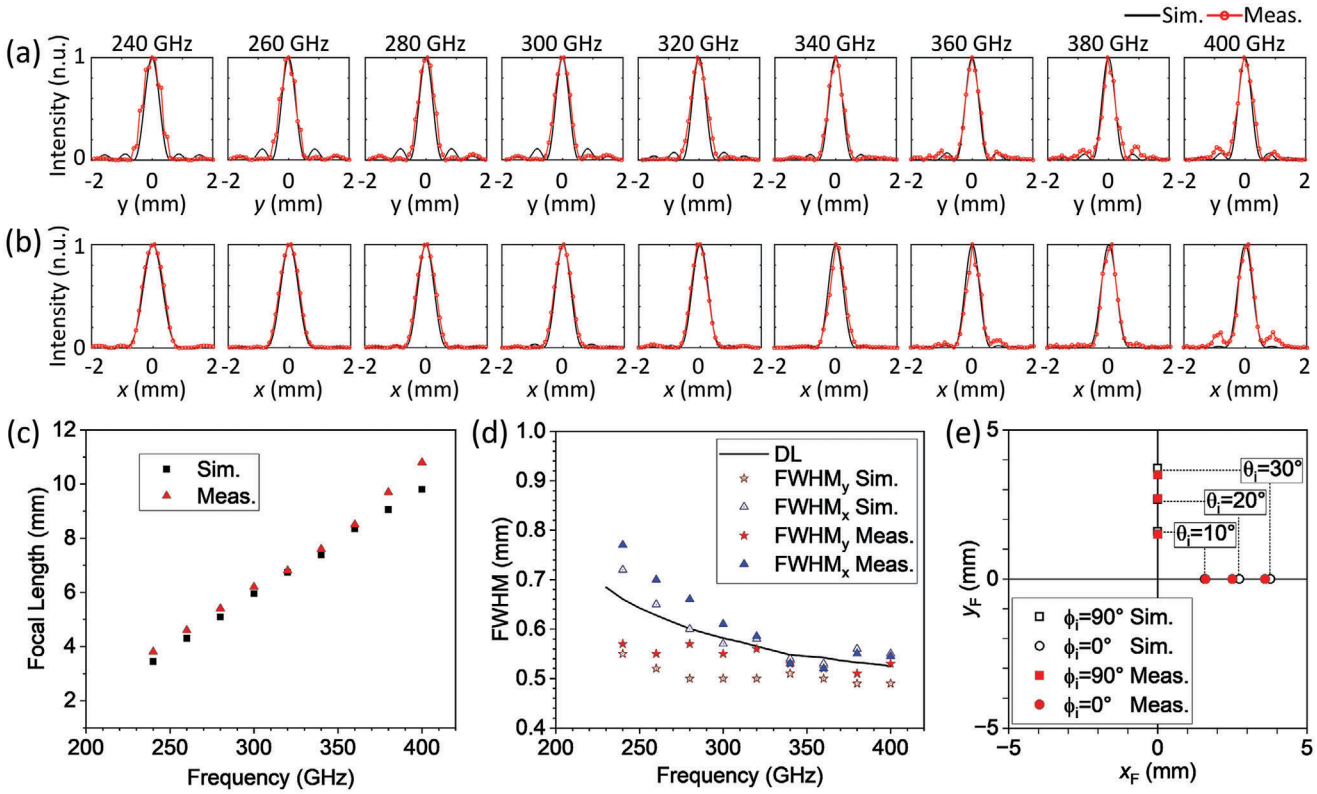

Figure 11. Comparison between the measured results and the simulated results. Normalized intensity distributions along the a) *y*-direction ($x = 0$) and b) *x*-direction ($y = 0$) on the focal plane. c) Focal lengths at different frequencies. d) FWHMs at different frequencies. e) Focal positions upon oblique incidences at 300 GHz.

Information, showing a rather high focusing efficiency of 33% achieved at 300 GHz.

4.2. Extension to Other Meta-Atoms and Meta-Devices

The metalens design method using aggressive discretization can potentially be used to design a plethora of broadband THz meta-devices at around 300 GHz. Various broadband unit cells exist, such as those based on X-pol modulation,[7,37,49] PB phase modulation,[28,50] and propagation phase modulation.[51] Besides, unit cell structures with multiple resonances (including the one in this paper) can be designed to achieve broadband performance by tuning the resonances.[36] These and more unit cell structures can be chosen according to the working polarization and desired performance, as long as the unit cell structure meets the conventional PCB fabrication standard. Additionally, our successful design of the broadband THz metalens (an aperiodic metasurface) shows that the design methodology can be used to design both periodic and aperiodic devices. Further, the co-polarized operation of the unit cells demonstrated in this work strongly suggests that independent control of both polarizations can be achieved, for example by tuning the *x*- and *y*-directed arms of the cross-shaped structure. Thus, the aggressive discretization method demonstrated in this paper can be broadly applied to construct many broadband THz meta-devices through PCB technology.

5. Conclusion

In conclusion, we have proposed a method for designing high quality THz metalenses which can be constructed from standard PCB fabrication. We have demonstrated in simulation and experiment that these metalenses can realize diffraction-limited focusing with large NA and broadband performance. Due to aggressive discretization, the metalenses are designed with the largest allowable unit cell size, leading to simple structures with relaxed feature sizes. This minimizes the fabrication difficulties in high frequency applications. Moreover, the enlarged element size allows the usage of weakly-resonant unit cell designs, resulting in broadband performance. With aggressive discretization, we design two metalenses with a unit cell size of $0.5\lambda_0$ at the design frequency of 300 GHz. First we design a single polarization metalens using a unit cell structure with three cascaded rectangular strips. Then we design a polarization-insensitive metalens using a unit cell structure with three cascaded cross-shaped patches. The proposed metalenses have a size of 20×20 mm^2 and a focal length of 6 mm at the design frequency, thus achieving a large NA of 0.86. They can achieve diffraction-limited focusing within a broad bandwidth of 240–400 GHz (a 50% bandwidth). Both metalenses are designed with a minimum line width and gap distance of 0.1 mm, which allows them to be fabricated using standard PCB technology. We have fabricated and measured the proposed metalenses, and reported focusing performances which agree very well with the simulation results. This work provides a solution

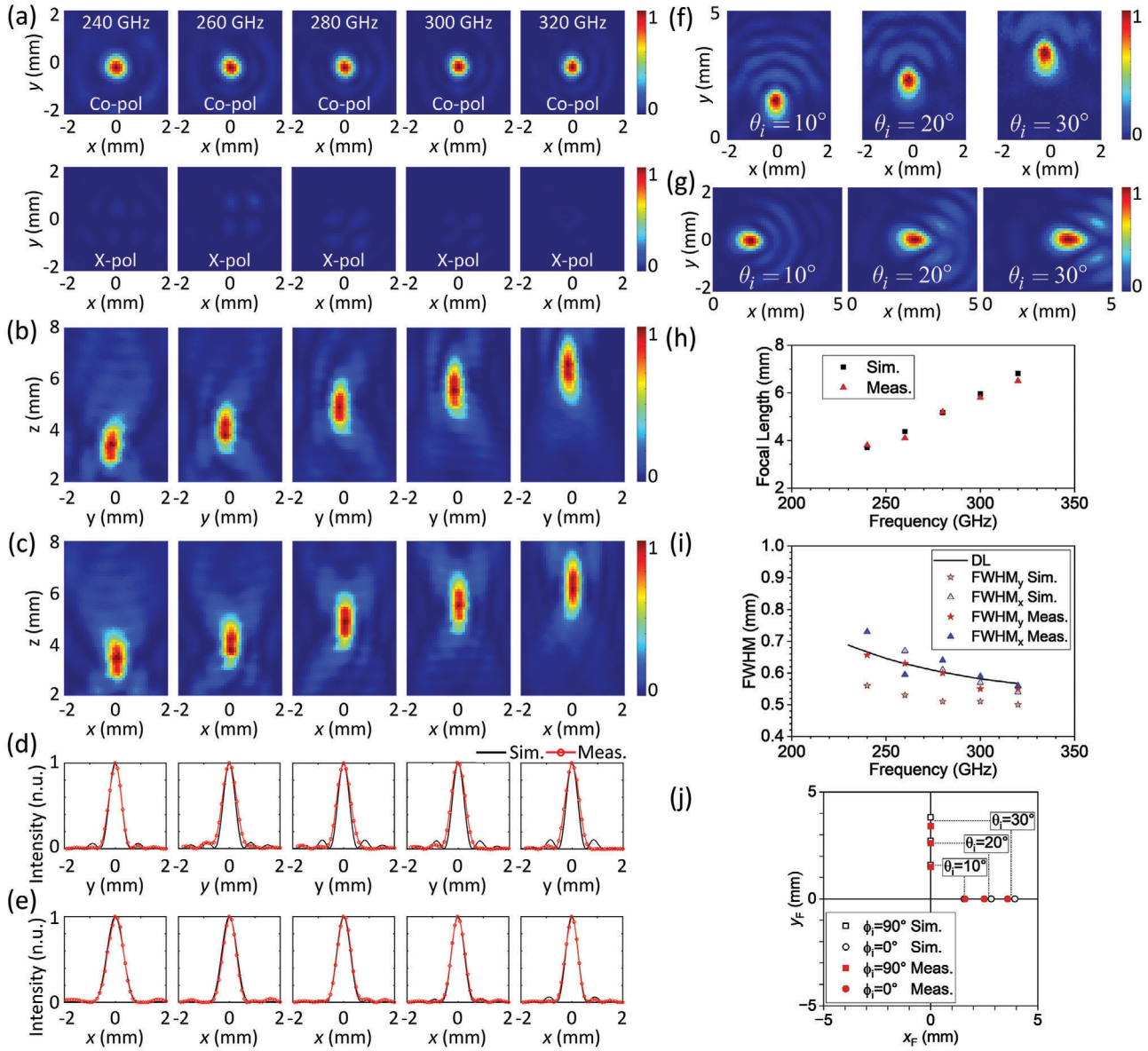

Figure 12. Measured results of the polarization-insensitive metalens. a–c) The normalized intensity distributions on a) the focal (*xy*) plane (*z* equals to the measured focal length as plotted in [h]), b) the *yz* plane ($x = 0$), c) the *xz* plane ($y = 0$) at different frequencies. d–e) Normalized intensity distributions along the d) *y*-direction ($x = 0$) and e) *x*-direction ($y = 0$) on the focal plane. f,g) The normalized intensity distributions on the focal (*xy*) plane ($z = 6$ mm) with oblique incidences with f) $\phi_i = 90°$ and g) $\phi_i = 0°$. h) Focal lengths at different frequencies. i) FWHMs at different frequencies. j) Focal positions upon oblique incidences at 300 GHz.

to THz meta-devices based on PCB technology, which is an established, fast, and cost-efficiency fabrication process compared to micro-fabrication and nano-fabrication technologies. Similar design methodology can be applied to other metasurfaces in the 300 GHz range, leading to mass-produced, cost-controlled PCB-based metasurfaces benefiting a plethora of applications in imaging and communication.

Supporting Information

Supporting Information is available from the Wiley Online Library or from the author.

Acknowledgements

This work was supported by a Collaborative Research Fund (Grant C6012-20G) and General Research Funds (CityU 21211619, CityU 11204522) from the Research Grants Council of Hong Kong.

Conflict of Interest

The authors declare no conflict of interest.

Data Availability Statement

The data that support the findings of this study are available from the corresponding author upon reasonable request.

Keywords

broadband, metalens, printed circuit boards, terahertz

Received: October 7, 2023
Revised: December 6, 2023
Published online:

[1] E. F. Kuester, M. A. Mohamed, M. Piket-May, C. L. Holloway, *IEEE Trans. Antennas Propag.* **2003**, *51*, 2641.
[2] C. L. Holloway, M. A. Mohamed, E. F. Kuester, A. Dienstfrey, *IEEE Trans. Electromagn. Compat.* **2005**, *47*, 853.
[3] L. Lin, X. M. Goh, L. P. McGuinness, A. Roberts, *Nano Lett.* **2010**, *10*, 1936.
[4] X. Ni, S. Ishii, A. V. Kildishev, V. M. Shalaev, *Light Sci. Appl.* **2013**, *2*, e72.
[5] A. Pors, M. G. Nielsen, R. L. Eriksen, S. I. Bozhevolnyi, *Nano Lett.* **2013**, *13*, 829.
[6] D. Lin, P. Fan, E. Hasman, M. L. Brongersma, *Science* **2014**, *345*, 298.
[7] Q. Wang, X. Zhang, Y. Xu, Z. Tian, J. Gu, W. Yue, S. Zhang, J. Han, W. Zhang, *Adv. Opt. Mater.* **2015**, *3*, 779.
[8] M. Khorasaninejad, W. T. Chen, R. C. Devlin, J. Oh, A. Y. Zhu, F. Capasso, *Science* **2016**, *352*, 1190.
[9] M. Khorasaninejad, A. Y. Zhu, C. Roques-Carmes, W. T. Chen, J. Oh, I. Mishra, R. C. Devlin, F. Capasso, *Nano Lett.* **2016**, *16*, 7229.
[10] M. Khorasaninejad, Z. Shi, A. Y. Zhu, W. T. Chen, V. Sanjeev, A. Zaidi, F. Capasso, *Nano Lett.* **2017**, *17*, 1819.
[11] S. Wang, P. C. Wu, V. C. Su, Y. C. Lai, C. Hung Chu, J. W. Chen, S. H. Lu, J. Chen, B. Xu, C. H. Kuan, T. Li, S. Zhu, D. P. Tsai, *Nat. Commun.* **2017**, *8*, 187.
[12] S. Larouche, Y. J. Tsai, T. Tyler, N. M. Jokerst, D. R. Smith, *Nat. Mater.* **2012**, *11*, 450.
[13] L. Huang, X. Chen, H. Mühlenbernd, H. Zhang, S. Chen, B. Bai, Q. Tan, G. Jin, K.-W. Cheah, C.-W. Qiu, J. Li, T. Zentgraf, S. Zhang, *Nat. Commun.* **2013**, *4*, 2808.
[14] X. Ni, A. V. Kildishev, V. M. Shalaev, *Nat. Commun.* **2013**, *4*, 2807.
[15] W. T. Chen, K. Y. Yang, C. M. Wang, Y. W. Huang, G. Sun, I. D. Chiang, C. Y. Liao, W. L. Hsu, H. T. Lin, S. Sun, L. Zhou, A. Q. Liu, D. P. Tsai, *Nano Lett.* **2014**, *14*, 225.
[16] Y. Yifat, M. Eitan, Z. Iluz, Y. Hanein, A. Boag, J. Scheuer, *Nano Lett.* **2014**, *14*, 2485.
[17] Y. W. Huang, W. T. Chen, W. Y. Tsai, P. C. Wu, C. M. Wang, G. Sun, D. P. Tsai, *Nano Lett.* **2015**, *15*, 3122.
[18] D. Wen, F. Yue, G. Li, G. Zheng, K. Chan, S. Chen, M. Chen, K. F. Li, P. W. Wong, K. W. Cheah, E. Y. Pun, S. Zhang, X. Chen, *Nat. Commun.* **2015**, *6*, 8241.
[19] R. C. Devlin, M. Khorasaninejad, W. T. Chen, J. Oh, F. Capasso, *Proc. Natl. Acad. Sci. U. S. A.* **2016**, *113*, 10473.
[20] Z. Yue, G. Xue, J. Liu, Y. Wang, M. Gu, *Nat. Commun.* **2017**, *8*, 15354.
[21] Z. L. Deng, J. Deng, X. Zhuang, S. Wang, K. Li, Y. Wang, Y. Chi, X. Ye, J. Xu, G. P. Wang, R. Zhao, X. Wang, Y. Cao, X. Cheng, G. Li, X. Li, *Nano Lett.* **2018**, *18*, 2885.
[22] X. Y. Jiang, J. S. Ye, J. W. He, X. K. Wang, D. Hu, S. F. Feng, Q. Kan, Y. Zhang, *Opt. Express* **2013**, *21*, 30030.
[23] D. Hu, X. Wang, S. Feng, J. Ye, W. Sun, Q. Kan, P. J. Klar, Y. Zhang, *Adv. Opt. Mater.* **2013**, *1*, 186.
[24] H. Liang, Q. Lin, X. Xie, Q. Sun, Y. Wang, L. Zhou, L. Liu, X. Yu, J. Zhou, T. F. Krauss, J. Li, *Nano Lett.* **2018**, *18*, 4460.
[25] W. T. Chen, A. Y. Zhu, V. Sanjeev, M. Khorasaninejad, Z. Shi, E. Lee, F. Capasso, *Nat. Nanotechnol.* **2018**, *13*, 220.
[26] K. Zhang, Y. Yuan, X. Ding, B. Ratni, S. N. Burokur, Q. Wu, *ACS Appl. Mater. Interfaces* **2019**, *11*, 28423.
[27] X. Jiang, H. Chen, Z. Li, H. Yuan, L. Cao, Z. Luo, K. Zhang, Z. Zhang, Z. Wen, L. G. Zhu, X. Zhou, G. Liang, D. Ruan, L. Du, L. Wang, G. Chen, *Opt. Express* **2018**, *26*, 14132.
[28] F. Zhao, Z. Li, X. Dai, X. Liao, S. Li, J. Cao, Z. Shang, Z. Zhang, G. Liang, G. Chen, H. Li, Z. Wen, *Adv. Opt. Mater.* **2020**, *8*, 2000842.
[29] M. Kang, Y. Ra'di, D. Farfan, A. Alù, *Phys. Rev. Appl.* **2020**, *13*, 044016.
[30] R. Wang, J. Han, J. Liu, H. Tian, W. Sun, L. Li, X. Chen, *Opt. Lett.* **2020**, *45*, 3506.
[31] Q. Yang, J. Gu, D. Wang, X. Zhang, Z. Tian, C. Ouyang, R. Singh, J. Han, W. Zhang, *Opt. Express* **2014**, *22*, 25931.
[32] Y. Q. Liu, J. Sun, Y. Che, K. Qi, L. Li, H. Yin, *Opt. Lett.* **2020**, *45*, 6262.
[33] Y.-Q. Liu, J. Sun, Y. Shu, L. Wu, L. Lu, K. Qi, Y. Che, L. Li, H. Yin, *Opt. Lasers Eng.* **2021**, *147*, 106734.
[34] Y.-Q. Liu, Y. Che, K. Qi, L. Li, H. Yin, *Opt. Commun.* **2020**, *474*, 126061.
[35] A. A. Fathnan, M. Liu, D. A. Powell, *Adv. Opt. Mater.* **2020**, *8*, 2000754.
[36] Q. Yang, J. Gu, Y. Xu, X. Zhang, Y. Li, C. Ouyang, Z. Tian, J. Han, W. Zhang, *Adv. Opt. Mater.* **2017**, *5*, 1601084.
[37] C. C. Chang, D. Headland, D. Abbott, W. Withayachumnankul, H. T. Chen, *Opt. Lett.* **2017**, *42*, 1867.
[38] A. Zhan, S. Colburn, R. Trivedi, T. K. Fryett, C. M. Dodson, A. Majumdar, *ACS Photonics* **2016**, *3*, 209.
[39] İ. A. Atalay, Y. A. Yilmaz, F. C. Savas, H. Kurt, *ACS Photonics* **2021**, *8*, 2481.
[40] A. Arbabi, Y. Horie, A. J. Ball, M. Bagheri, A. Faraon, *Nat. Commun.* **2015**, *6*, 7069.
[41] Z.-P. Zhuang, R. Chen, Z.-B. Fan, X.-N. Pang, J.-W. Dong, *Nanophotonics* **2019**, *8*, 1279.
[42] F. Zhang, H. Yu, J. Fang, M. Zhang, S. Chen, J. Wang, A. He, J. Chen, *Opt. Express* **2016**, *24*, 6656.
[43] H. Zhang, X. Zhang, Q. Xu, C. Tian, Q. Wang, Y. Xu, Y. Li, J. Gu, Z. Tian, C. Ouyang, X. Zhang, C. Hu, J. Han, W. Zhang, *Adv. Opt. Mater.* **2018**, *6*, 1700773.
[44] H. Chen, Z. Wu, Z. Li, Z. Luo, X. Jiang, Z. Wen, L. Zhu, X. Zhou, H. Li, Z. Shang, Z. Zhang, K. Zhang, G. Liang, S. Jiang, L. Du, G. Chen, *Opt. Express* **2018**, *26*, 29817.
[45] D. Jia, Y. Tian, W. Ma, X. Gong, J. Yu, G. Zhao, X. Yu, *Opt. Lett.* **2017**, *42*, 4494.
[46] C. Qi, A. M. H. Wong, *IEEE Trans. Antennas Propag.* **2022**, *70*, 7300.
[47] F. Aieta, P. Genevet, M. A. Kats, N. Yu, R. Blanchard, Z. Gaburro, F. Capasso, *Nano Lett.* **2012**, *12*, 4932.
[48] E. Abbe, *Arch. Mikrosk. An'at.* **1873**, *9*, 413.
[49] X. Jiang, W. Fan, C. Qin, X. Chen, *Nanomaterials* **2021**, *11*, 2895.
[50] Q. Cheng, M. Ma, D. Yu, Z. Shen, J. Xie, J. Wang, N. Xu, H. Guo, W. Hu, S. Wang, *Sci. Bull.* **2019**, *64*, 1525.
[51] Y. Xu, J. Gu, Y. Gao, Q. Yang, W. Liu, Z. Yao, Q. Xu, J. Han, W. Zhang, *Adv. Funct. Mater.* **2023**, *33*, 2302821.